Materials Science in Semiconductor Processing 26 (2014) 7–17

Contents lists available at ScienceDirect

Materials Science in Semiconductor Processing

journal homepage: www.elsevier.com/locate/mssp

Comparison of the photocatalytic degradation of trypan blue by undoped and silver-doped zinc oxide nanoparticles

T.N. Ravishankar [a], K. Manjunatha [a], T. Ramakrishnappa [a], G. Nagaraju [a,b,*], Dhanith Kumar [b], S. Sarakar [c], B.S. Anandakumar [d], G.T. Chandrappa [d], Viswanath Reddy [e], J. Dupont [f]

[a] Centre for Nano and Material Sciences, Jain University, Jakkasandra, Kanakapura (T), India
[b] Department of Chemistry, BMS Institute of Technology, Bangalore, India
[c] Department of Inorganic and Physical Chemistry, Indian Institute of Science, Bangalore, India
[d] Department of Chemistry, Central College Campus, Bangalore University, Bangalore, India
[e] Liquid Crystal Research Center, Department of Chemistry, Hull University, Hull, United Kingdom
[f] Laboratory of Molecular Catalysis, Institute of Chemistry, UFRGS, Porto Alegre, Brazil

ARTICLE INFO

Keywords:
Silver doped zinc oxide
Combustion
Trypan blue
Optical properties
Degradation

ABSTRACT

Zinc oxide (ZnO) and silver doped zinc oxide (ZnO:Ag) nanoparticles were prepared using nitrates of zinc and silver as oxidizers and ethylene diaminetetraacetic acid (EDTA) as a fuel via low-temperature combustion synthesis (LCS) at 500 °C. X-ray diffraction (XRD) pattern indicates the presence of silver in the hexagonal wurtzite structure of ZnO. Fourier transform infrared (FTIR) spectrum indicates the presence of Ag–Zn–O stretching vibration at 510 cm^{-1}. Transmission electron microscopy (TEM) images shows that the average particle size of ZnO and ZnO:Ag nanoparticles were found to be 58 nm and 52 nm, respectively. X-ray photoelectron spectroscopy (XPS) data clearly indicates the presence of Ag in ZnO crystal lattice. The above characterization techniques indicate that the incorporation of silver affects the structural and optical properties of ZnO nanoparticles. ZnO:Ag nanoparticles exhibited 3% higher photocatalytic efficiency than pure ZnO nanoparticles. ZnO:Ag nanoparticles show better photocatalytic activity for the degradation of trypan blue (TrB) compared to undoped ZnO nanoparticles.

1. Introduction

Nanocrystalline transition metal oxides have attracted wide attention due to their unique properties, which are technologically very useful in nano-device fabrications [1,2]. Amongst these materials, zinc oxide (ZnO) nanoparticles were very interesting due to their semiconducting property with a band gap of 3.370 eV, a relatively high excitation binding energy (60 meV) and unique properties like promising photocatalyst, excellent piezoelectric and novel optical properties [3]. Various groups have used doped and undoped ZnO nanoparticles as photocatalyst for the degradation of organic dye. They found that undoped ZnO exhibited lower photocatalytic activity than the doped ZnO nanomaterials. This is because in pure ZnO the rate of electron–hole pair recombination is more than the doped ZnO nanomaterials [4,5]. Therefore, in order to enhance the photocatalytic activity of ZnO nanoparticles, noble metal incorporation, coupling with other semiconductors or by adding adsorbent to the ZnO have been carried out by various groups around the world [6,7]. Of these, noble metal ion incorporation have been studying extensively and proved to be very effective in improving the photocatalytic activity and also to tune the optical and electrical properties of ZnO [8]. Various groups

* Corresponding author. Tel.: +91 80 27506270.
E-mail address: nagarajugn@rediffmail.com (G. Nagaraju).

http://dx.doi.org/10.1016/j.mssp.2014.03.027
1369-8001/

have synthesized ZnO:Ce nanoparticles [9], ZnO:Pd nanoparticles [10], ZnO:Al nanoparticles [11], and ZnO:Mn nanoparticles [12] by different method and observed the improved performance compared to pure ZnO nanoparticles. Literature surveys suggested that ZnO or ZnO:Ag is non-toxic in nature and are used in the various biological/medical applications [13]. However, inhalation or consumption of large quantity of ZnO or ZnO:Ag through food additives, synthesis or through any other way causes severe damages to living cells (olfactory epithelium) as reported by Gao et al. [14]. Mohamad reported that the consumption of ZnO nanoparticles causes liver problems [15]. Bondarenko et al. reported the in-vitro toxicity of ZnO:Ag nanoparticles on mammalian cells [16]. Literatures survey suggested that the ZnO and ZnO:Ag nanoparticles are physically and chemically stable. Susan et al. reported the synthesis of ZnO:Ag heterostructure nanoparticles for antibacterial and thermal studies. They observed that ZnO:Ag nanoparticles significantly increased the thermal stability of cellulose nanocrystals [17]. Rahman et al. observed that starch-based polymer ZnO nanoparticles show improved dielectric and conductive properties compared to pure ZnO nanoparticles [18]. Altıntas Yıldırım et al. synthesized ZnO:Ag nanoparticles at room temperature and found ZnO:Ag better than ZnO with respect to optical properties [19]. Teng et al. found vertically aligned ZnO:Ag nanowires arrays for photo electrochemical applications better than bare ZnO nanoparticles [20]. Ozlem et.al [21] and Shah et.al [22] also observed similar improved photocatalytic and antibacterial activity in synthesized ZnO:Ag nanoparticles. From all the above-stated literature, it is clear that Ag is one of the most promising dopant which alters the surface and fabrication of ZnO by decreasing the total volume of the particle which in turn, decreases the recombination probability making more carriers available for the oxidation/reduction on the surface [23]. The surface area and surface defects play an important role in photocatalytic activities of ZnO [24–26]. Various methods are available to prepare ZnO:Ag nonstructural materials, a few of them are co-precipitation [27], hydrothermal [28], sol–gel method [29], electro deposition [30], solution combustion method [31] etc. Amongst the available methods, solution combustion method is considered simple, instantaneous, single-step and energy-saving. This method also produces homogenous, very fine crystalline product without intermediate calcinations or grinding [32,33]. Here we report the synthesis of ZnO:Ag nanoparticles using nitrates of Zn and Ag as an oxidizers and ethylene diaminetetraacetic acid (EDTA) as a fuel by the low temperature combustion synthesis (LCS) method. EDTA is used as fuel because it is nontoxic, low cost, and rich in carbon, nitrogen, hydrogen and oxygen which are released as their corresponding gases during combustion. The release of these gases leads to the formation of highly porous, voluminous and high-surface area ZnO:Ag nanoparticles. The obtained product shows good photocatalytic activity which has been studied using trypan blue, a toxic azo dye. Trypan blue has been used extensively in the textile, food and paints industries for dyeing nylon, wool, cotton, silk and also for coloring of oil, fats, waxes, varnish, plastics, etc. Dyes create several environmental problems by releasing highly carcinogenic molecules into the aqueous medium. Various techniques have been used for the removal of dyes from the aqueous medium like biodegradation and photocatalytic degradation. Reviewing the available literature indicated that the biodegradation method cannot be used to degrade azo dyes [34]. Researchers show inclination towards photocatalytic degradation these days because the reactions are carried out under ambient conditions. The structure of dye can be shown in Fig. 1.

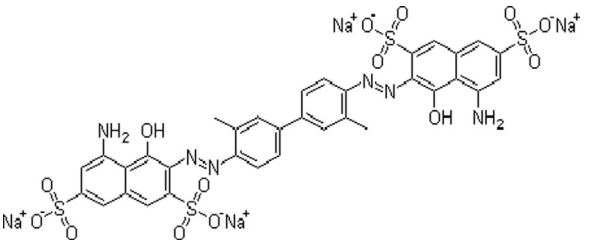

Fig. 1. Structure of trypan blue dye.

2. Experimental method

2.1. Preparation of ZnO and Ag doped ZnO nanoparticles

In order to prepare ZnO and ZnO:Ag nanoparticles, nitrates of zinc and silver are used as oxidizers and EDTA as fuel. To remove the sodium ions from the salt, the disodium salt of EDTA is treated with 2 M HCl solution (Fig. 2). The obtained precipitate (EDTA) is washed several times with water to remove sodium ions and dried at 100 °C for 1 h. The dried EDTA is used as fuel for the preparation of ZnO and ZnO:Ag nanoparticles. Stoichiometric amounts of nitrates of zinc and silver as oxidizers and fuel (EDTA) in 1:1 ratio are taken in a trough; required amount of double distilled water is added. A good combination of fuel and oxidizer is one which is completely soluble in water to form homogenous redox solution. EDTA is sparingly soluble in cold water and completely soluble in hot water. The homogeneous redox solution is pre-heated on a hot plate at 150 °C, until it forms gel on dehydration. This gel is introduced into a preheated muffle furnace maintained at 500 °C; smoldering type of combustion takes place and within 3–4 min, the reaction proceeds to completion and forms nanocrystalline ZnO. The products were calcined at 500 °C for 1 h. The same procedure is followed for the preparation of ZnO:Ag nanoparticles where the ratio is 1:0.5:1 (zinc nitrate:silver nitrate:EDTA).

2.2. Characterization

X-ray diffraction (XRD) data were recorded on Philips X'pert PRO X-ray diffractometer with graphite monochromatized Cu-Kα (1.542 Å) radiation. X-ray photoelectron spectroscopy (XPS) analysis was carried out on an ESCALAB 250 (Thermo-VG Scientific), using Al Kα as the excitation source. The instrument was standardized against the C1s spectral line at 284.600 eV. The Fourier transform infrared spectra (FTIR) of the samples were collected using Bruker Alpha-P spectrometer. The absorption spectra of the samples were measured on a Perkin Elmer Lambda-750 UV–vis spectrometer (Ultraviolet–visible). Photoluminescence (PL) spectra were examined by Perkin Elmer spectrometer using Xe lamp with an

excitation wavelength of 330 nm. The surface morphology was observed using Carl Zeiss ultra 55 scanning electron microscopy (SEM). Transmission electron microscopy (TEM) was performed JEOL JEM 1200 Ex operating at 100 kV. The surface areas of the samples were analyzed by Smart Sorb/93 Brunauer, Emmett and Teller (BET) surface analyzer (with sorb93 reduction software) and fluorescence intensity was measured by spectro-flurophotometer (Shimadzu, RF-5301PC Series).

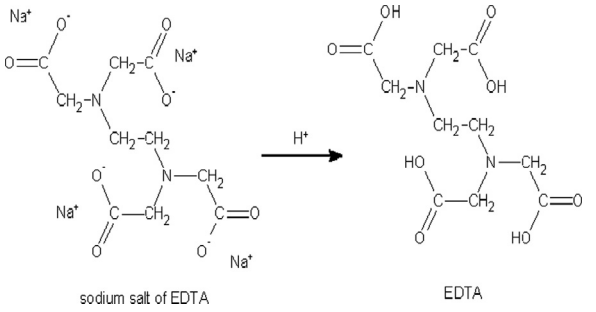

Fig. 2. Conversion of sodium salt of EDTA to EDTA.

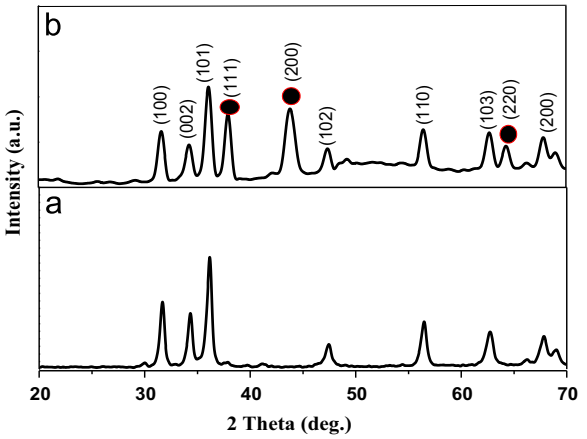

Fig. 3. (a) PXRD pattern of the ZnO and (b) ZnO:Ag nanoparticles.

2.3. Experimental procedure for photocatalytic degradation of dye

Photocatalytic experiments were carried out in a $150 \times 75\ mm^2$ batch reactor. A catalytic load of 100 mg in 100 mL of the dye was prepared. The pH of the solution was adjusted by addition of either 0.050 M NaOH or 0.050 M H_2SO_4. The slurry composed of dye solution and catalyst was placed in the reactor and stirred magnetically for agitation with simultaneous exposure to sun light/UV light. Known volume of the slurry was withdrawn at specific interval of time, centrifuged to remove the interference of the catalyst and assessed using spectrophotometer (592 nm) for rate of degradation. The % of degradation can be determined using the following formula shown in the Eq. (1).

$$\%\ \text{of degradation} = \frac{C_i - C_f}{C_i} \times 100 \quad (1)$$

C_i and C_f are the initial and final concentrations of dye. The experiment was carried out by varying experimental parameters like concentration of dye, catalytic load, irradiation time, pH and nature of light.

3. Result and discussion

Fig. 3 shows the XRD pattern of the ZnO and ZnO:Ag nanoparticles. XRD was used to check the purity, crystallinity of the nanocrystals and also to detect the presence of Ag. In Fig. 3(a) all the diffraction peaks of the product can be indexed to hexagonal wurtzite structure with lattice points $a=b=3.253$ Å and $c=5.213$ Å (JCPDS no. 89-1397). The crystallite size calculated from most intense peaks ($2\theta=36.300^\circ$) by Scherrer's formula was found to be ~45 nm. Fig. 3(b) depicts the XRD pattern of ZnO:Ag

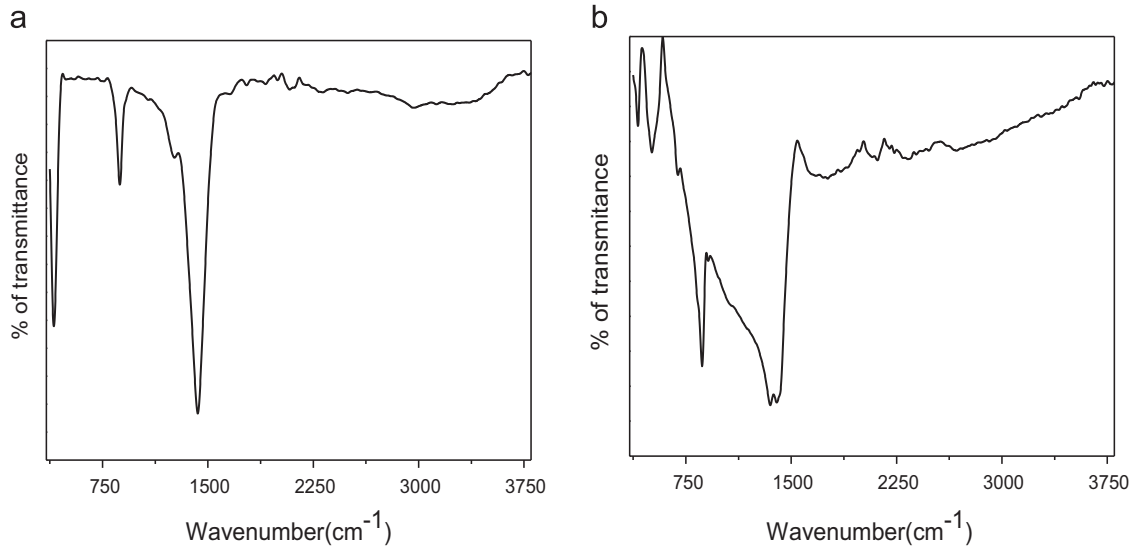

Fig. 4. (a) FTIR spectrum of the ZnO and (b) ZnO:Ag nanoparticles.

nanoparticles. It was found that in addition to the hexagonal wurtzite ZnO structure, the diffraction peaks at two theta values 37.900, 43.800 and 64.300can be assigned to cubic-phase Ag (JCPDS no.4-783) [20]. This clearly indicates the presence of Ag in ZnO crystal lattice. The crystallite size calculated from most intense peak ($2\theta = 36.1^{\circ}$) by Scherrer's formula was found to be at ~40 nm. FTIR spectra of un-doped and doped ZnO nanoparticles are shown in Fig. 4(a) and (b) respectively. A broad peak at ~3336 cm^{-1} (Fig. 4(a)) indicates the presence of hydroxyl residue which is due to the atmospheric moisture [35,36]. The spectral region from 850 to 1450 cm^{-1} shows the presence of carbonated impurities [37].

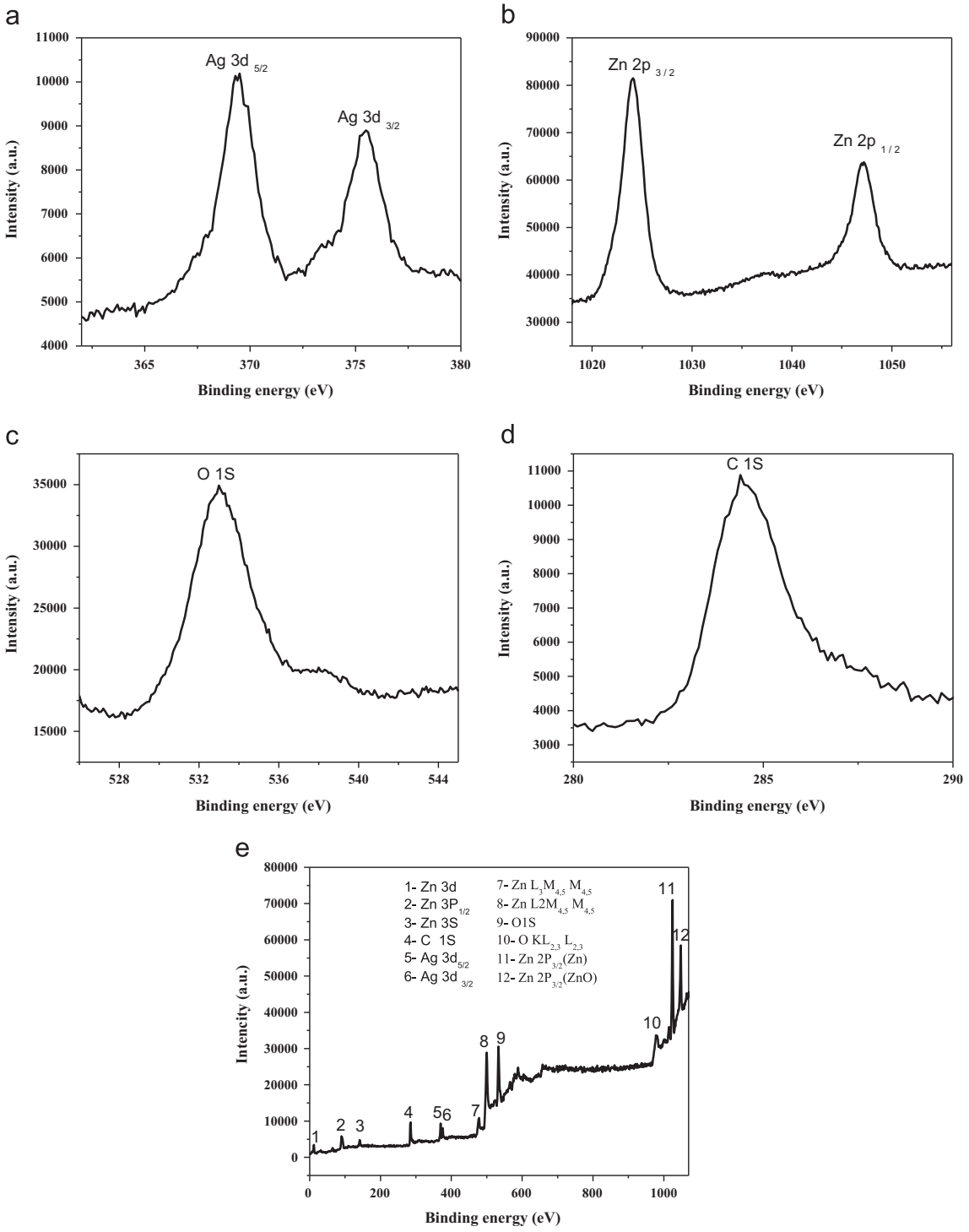

Fig. 5. (a) XPS spectra of Ag, (b) Zn, (c) O, (d) C and (e) wide spectrum of ZnO:Ag nanoparticles.

A peak at 408 cm^{-1} is associated with the characteristic vibrational mode of Zn–O bond [38,39]. Significant spectroscopic (Fig. 4(b)) bands at 405 cm^{-1} and 510 cm^{-1} can be assigned to Zn–O and Ag–ZnO vibrational stretching frequencies respectively [40–43]. XPS spectra of Ag 3d, Zn 2p, O 1s, C1s and wide spectrum of ZnO:Ag is shown in Fig. 5. XPS measured at the Ag 3d core levels (Fig. 5 (a)), i.e., Ag 3d 5/2 and Ag 3d 3/2 binding energies appeared at 369 eV and 375 eV, respectively. This is in good agreement with metallic silver values [44,45]. XPS spectrum of Zn 2p (Fig. 5(b)), shows two peaks at 1024 eV for Zn 2p3/2 corresponds to the hydroxyl groups attached to the Zn ions on the surface of nanoparticles [46]. Another peak at 1044.200 eV corresponds to Zn atoms bonded to oxygen atoms to form ZnO instead of Zn–C–O alloys [47]. XPS spectrum of O1s (Fig. 5(c)) shows strong peak at 530.200 eV which is the characteristic of lattice oxygen in ZnO:Ag [48]. XPS spectrum of C1s is shown in Fig. 5(d). It shows strong peak ~284.300 eV which can be assigned to C–O groups [49]. The overall XPS spectrum of ZnO:Ag nanoparticles are as shown in Fig. 5(e) where all the peaks observed in the spectrum were in agreement with the earlier reports [50].

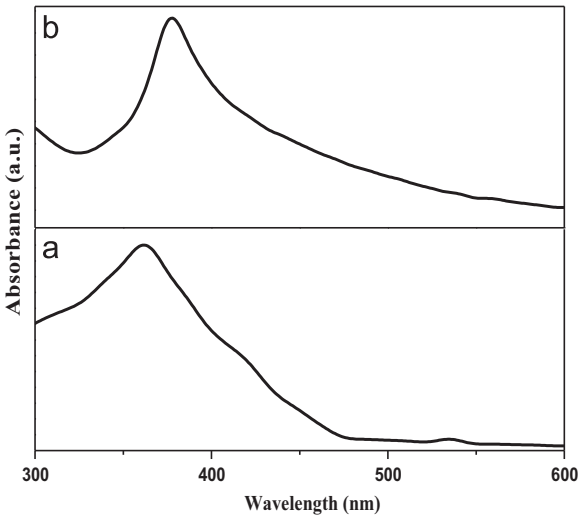

Fig. 6. (a) UV–visible spectrum of the ZnO and (b) ZnO:Ag nanoparticles.

Fig. 6 shows the UV–vis spectra of the ZnO and ZnO:Ag nanoparticles. Pure ZnO nanoparticles (Fig. 6(b)) show a maximum absorbance at 360 nm corresponding to a band gap of 3.460 eV which was blue shifted compared to that of bulk ZnO nanoparticles (3.370 eV). The blue shift may be due to quantum size effects, [51]. Fig. 6(b) shows the maximum absorbance at 378 nm corresponding to a band gap of 3.100 eV, which was red shifted compared to undoped as well as bulk ZnO. It clearly indicates that Ag was successfully inserted into the ZnO crystal lattice. This indicates that ZnO:Ag nanoparticles have much stronger absorption than that of ZnO nanoparticles, i.e., ZnO:Ag nanoparticles possess higher photocatalytic activity than undoped ZnO nanoparticles [52]. Fig. 7(a) and (b) showed the room temperature PL spectrum of the both undoped and doped ZnO nanoparticles respectively. Both the spectra showed a strong, broad UV emission at 380 nm, which comes from the band edge recombination of free excitation [53] and sharp peak at 512 nm, has been assigned to oxygen vacancy 'Vo' and substitution defects [54]. SEM images of ZnO and ZnO:Ag nanoparticles (Fig. 8(a) and (b)) show that the nanoparticles are agglomerated during the formation stage itself to form very tiny crystals. Fig. 8(c) and (d) clearly shows the presence of bright Ag nanoparticles on the surface of ZnO. TEM images (Fig. 9) showed irregular sized, almost spherical shaped nanoparticles with average size 58 nm and 52 nm for undoped and doped ZnO nanoparticles respectively. BET surface area of the ZnO and ZnO:Ag nanoparticles were found to be 40.110 m^2/g and 71.210 m^2/g respectively. It is clear from BET studies that ZnO:Ag has a higher surface area, hence enhanced photocatalytic activity.

3.1. *Photocatalytic activity of ZnO and ZnO:Ag nanoparticles*

3.1.1. *Effect of dye concentration*

Fig. 10 shows the effect of dye concentration on the photocatalytic activity of ZnO and ZnO:Ag nanoparticles.

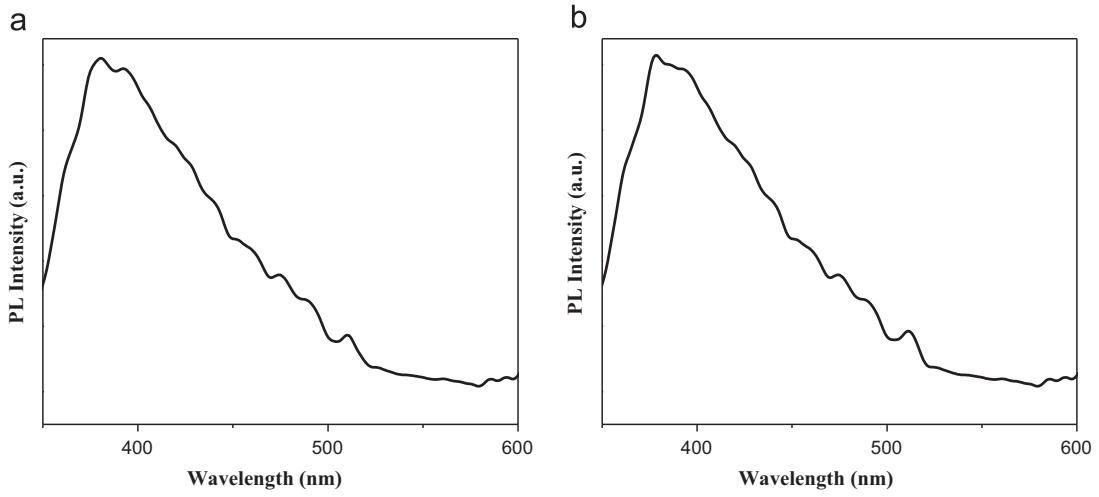

Fig. 7. (a) Photoluminescence spectrum of the ZnO and (b) ZnO:Ag nanoparticles.

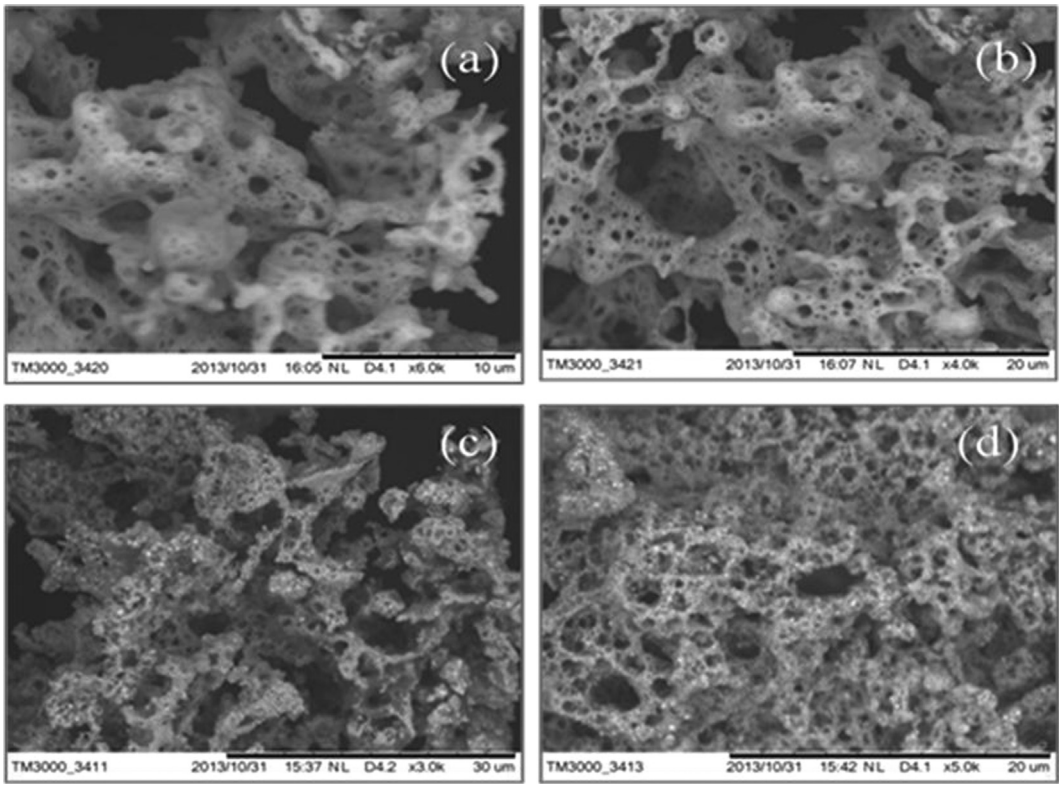

Fig. 8. (a) and (b) SEM images of the ZnO and (c) and (d) ZnO:Ag nanoparticles.

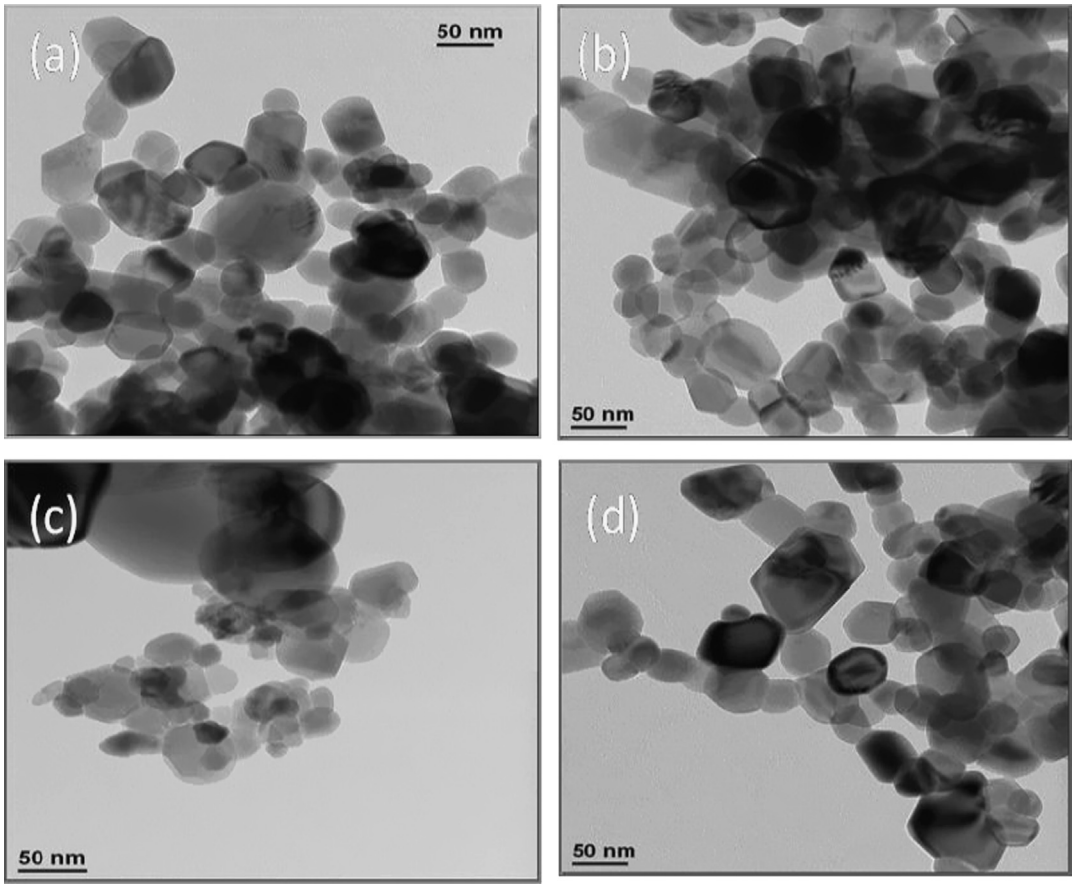

Fig. 9. (a) and (b) TEM images of the ZnO and (c) and (d) ZnO:Ag nanoparticles.

Experimental parameters are, concentration of trypan blue (TrB): 5–25 μg/L, amount of catalyst: 100 mg/100 mL and pH: 10. As the concentration of dye increases, time taken for complete degradation increases. At increased concentrations more dye molecules are adsorbed on to the surface of catalyst resulting in decreased active sites on the catalyst (lesser number of hydroxyl and superoxide radicals) and thereby, reduced light penetration. ZnO and ZnO:Ag nanoparticles degrade 5 μg/L dye solution completely after 120 min and 90 min of illumination respectively, whereas for 25 μg/L dye solution degradation efficiency is 70% (Fig. 10(a)) and 80% (Fig. 10(a)) after 120 min for ZnO and ZnO:Ag, respectively.

3.1.2. Effect of catalyst dose

Effect of catalytic load on the photocatalytic degradation of dye is shown in Fig. 11. In order to determine the optimal dosage of the catalysts; the catalytic load was varied from 0.250 mg/100 mL to 1.500 mg/100 mL. The optimized load was found to be 1.250 mg/100 mL. Below this optimum load, active sites on the surface of the catalyst increases resulting in rapid degradation. Above the optimum load, turbidity of the slurry increases, light penetration decreases and thus, availability of hydroxides and super oxides become minimal. Fig. 11(a) and (b) shows that 1.250 mg/100 mL of dye solution degraded completely at 90 min and 75 min for ZnO and ZnO:Ag nanoparticles respectively.

3.1.3. Effect of pH on photocatalytic degradation

The pH of a dye solution is very important for degradation and is as shown in Fig. 12. From the figure it is clear that photocatalytic degradation efficiency is more in basic condition than in acidic condition. This observation matches well with the reported studies [55,56]. The variation of pH alters the surface properties of ZnO and ZnO:Ag nanoparticles, in turn, dissociation of the dye molecules. At pH 10, perhydroxyl radicals are formed, leading to the formation of hydrogen peroxide which gives more number of hydroxyl radicals. The highest photocatalytic degradation observed in both the cases is at pH 10. Mechanisms of formation of possible radicals are as shown in Eqs. (2)–(11).

$$O_2 + e^- \rightarrow O_2^{\bullet -} \quad (2)$$

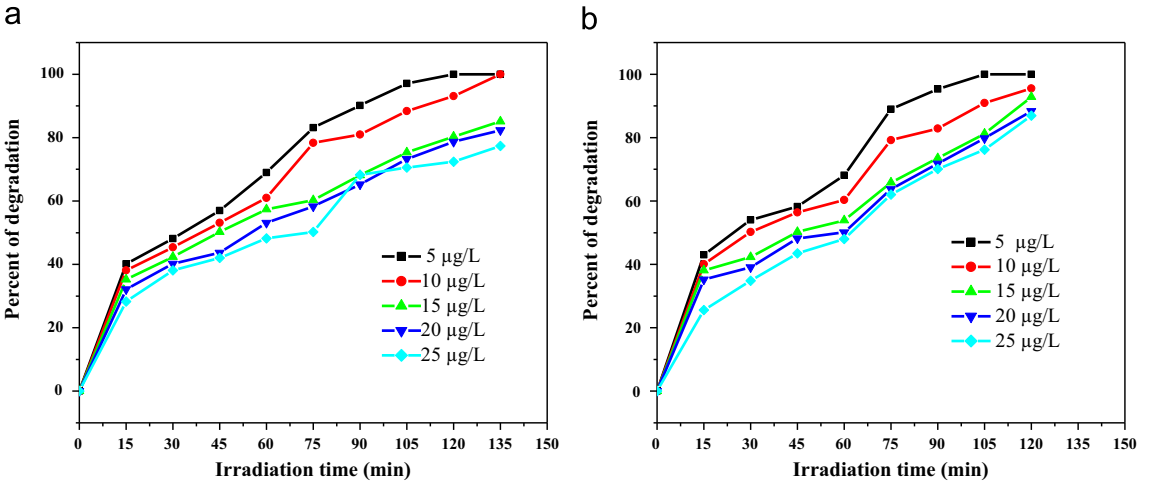

Fig. 10. (a) Effect of dye concentration on the photocatalytic process of the ZnO and (b) ZnO:Ag nanoparticles.

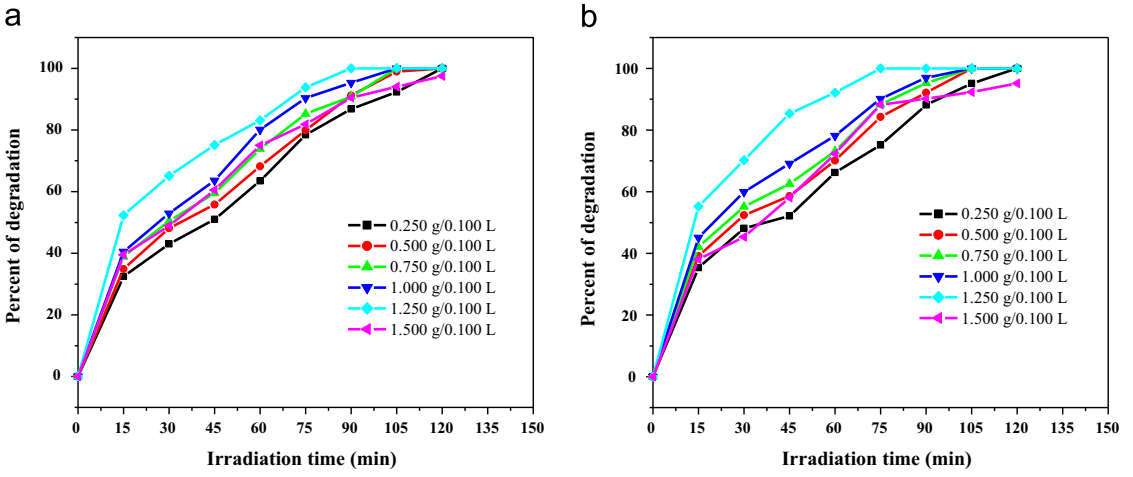

Fig. 11. (a) Effect of catalytic load on the photocatalytic process of the ZnO and (b) ZnO:Ag.

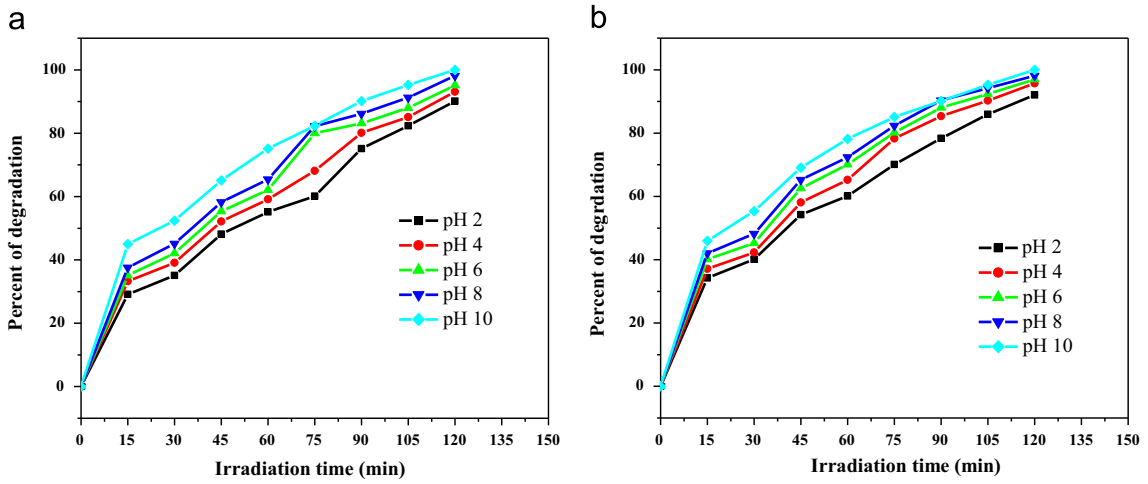

Fig. 12. (a) Effect of pH on photocatalytic process of the ZnO and (b) ZnO:Ag nanoparticles.

$$O_2^{\bullet -} + H^+ \rightarrow HO_2\cdot \quad (3)$$

$$HO_2\cdot + HO_2\cdot \rightarrow H_2O_2 + O_2 \quad (4)$$

$$H_2O_2 + e_{cb}^- \rightarrow HO^{\bullet} + HO^- \quad (5)$$

$$H_2O_2 + O_2\cdot \rightarrow HO^{\bullet} + HO^- + O_2 \quad (6)$$

$$H_2O_2 \rightarrow 2HO^{\bullet} \quad (7)$$

$$O_2 + HO^- \rightarrow O_2\cdot + HO^{\bullet} \quad (8)$$

$$\text{Dye} + OH \rightarrow \text{degradation products} \quad (9)$$

$$\text{Dye} + h_{VB^+} \rightarrow \text{oxidation products} \quad (10)$$

$$\text{Dye} + e_{CB^-} \rightarrow \text{reduction products} \quad (11)$$

3.1.4. Comparative study of photocatalytic activity of ZnO and ZnO:Ag nanoparticles

Fig. 13 shows the comparative study of photocatalytic activity of ZnO and ZnO:Ag nanoparticles. Photocatalytic reaction was carried out at constant dye concentration (5 μg/L) and catalytic load (500 mg/100 mL) at pH 10. The above experiment clearly indicates that the photocatalytic activity of ZnO:Ag nanoparticles were superior to ZnO nanoparticles [57].

3.1.5. Determination of quantum yield of ZnO and ZnO:Ag nanoparticles

Quantum yield or photonic efficiency of the photocatalyst is studied using UV–visible spectrometer and spectro-flurophotometer. Quinine sulfite is used as standard and quantum yield can be calculated by the formula

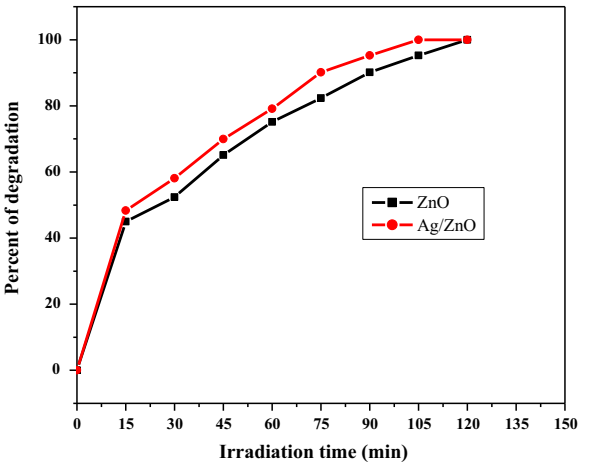

Fig. 13. Comparison study of photocatalytic activity of undoped and ZnO:Ag nanoparticles.

Table 1
Absorbance and integrated fluorescence intensity of quinine sulfite.

Absorbance	Integrated fluorescence intensity
0.201	15946.518
0.295	2222.754
0.409	30019.625
0.500	37803.570
0.598	45428.728
0.710	55759.227

as shown in the Eq. (12).

$$Q_{\text{unknown}} = \frac{Q_{\text{known}} \times (\text{Slope})\,\text{unknown} \times \eta^2\text{unknown}}{(\text{Slope})_{\text{known}} \times \eta^2\text{known}} \quad (12)$$

Q is quantum yield, η is refractive index of solvent used and slope can be calculated by plotting absorbance vs integrated fluorescence intensity. The quantum yield of ZnO photocatalyst is 0.616 and the quantum yield of ZnO:Ag photocatalyst is 0.634 i.e. photocatalytic efficiency of ZnO:Ag is 3% higher than that of the bare ZnO nanoparticles [58]. Absorbance,

Table 2
Absorbance and integrated fluorescence intensity of ZnO photocatalyst.

Absorbance	Integrated fluorescence intensity
0.060	17881.857
0.236	28269.217
0.313	41010.281
0.537	65103.938
0.698	75177.632
0.815	85901.147

Table 3
Absorbance and integrated fluorescence intensity of ZnO:Ag photocatalyst.

Absorbance	Integrated fluorescence intensity
0.052	15570.726
0.140	28842.163
0.270	42318.405
0.400	54811.578
0.548	63331.578
0.748	78487.165

integrated fluorescence intensity of quinine sulfite, ZnO, and ZnO:Ag nanoparticles are shown in Tables 1–3 respectively. Graph of absorbance vs integrated fluorescence intensity of quinine sulfite, ZnO, and ZnO:Ag nanoparticles are shown in Fig. 14(a)–(c) correspondingly.

3.1.6. Determination of adsorption equilibrium of TrB on the nanoparticles surfaces

In order to investigate the adsorption and absorption equilibria of TrB on the surfaces of ZnO and ZnO:Ag nanoparticles, the reaction was carried out in dark. The concentration of dye is varied from 5 to 25 μg/L, catalytic load is 1.250 mg/100 mL and pH of the solution is 10. The suspensions are allowed to attain equilibrium in the dark under continuous stirring. The slurry is withdrawn for every 30 min (10 mL), and then centrifuged. The absorbance of the supernatant was measured to determine the concentration of dye and the experimental results are shown in Fig. 15. We noticed that the adsorption and absorption equilibria of TrB on the surfaces of ZnO and ZnO:Ag nanoparticles are found to be 60 min and 65 min,

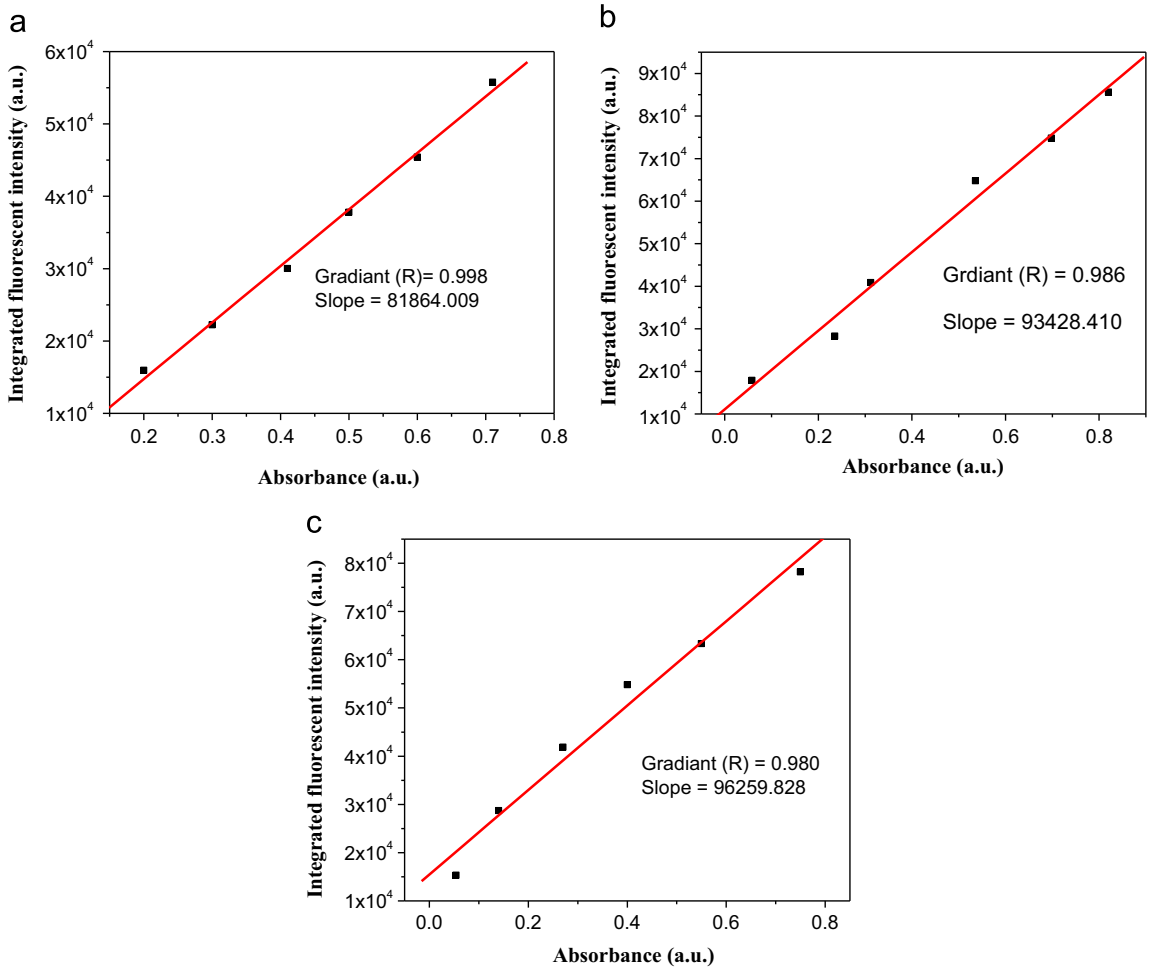

Fig. 14. (a) Graph of absorbance vs integrated fluorescence intensity of quinine sulfite, (b) ZnO and (c) ZnO:Ag nanoparticles.

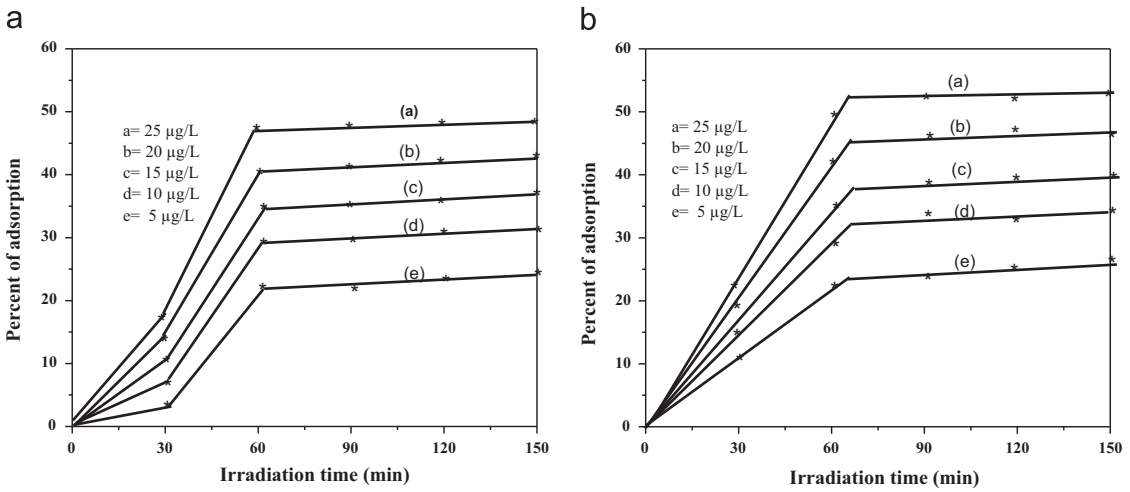

Fig. 15. (a) Adsorption and absorption behavior of dye on the surface of ZnO and (b) ZnO:Ag.

respectively. Beyond this time the dye could not be degraded [59].

4. Conclusion

We have successfully synthesized ZnO and ZnO:Ag nanoparticles via the low temperature solution combustion method. PXRD pattern of doped ZnO clearly shows the presence of Ag in the ZnO matrix. FTIR shows a band at 405 cm^{-1} and 510 cm^{-1} due to Zn–O and Ag–ZnO vibrational stretching. XPS data clearly shows the incorporation of Ag into the ZnO crystal lattice. UV–vis absorption spectrum of ZnO:Ag nanoparticles show red shift compared to the undoped ZnO nanoparticles. PL spectrum of the ZnO and ZnO:Ag nanoparticles showed a strong UV emission at around 380 nm. TEM images showed that nanoparticles are almost spherical in shape and the average size of the ZnO:Ag particles were found to be 52 nm. ZnO:Ag nanoparticles possess higher surface area than the ZnO nanoparticles. ZnO:Ag nanoparticles show very good photocatalytic activity than bare ZnO nanoparticles for the degradation of trypan blue dye.

Acknowledgment

One of the authors, Ravishankar T.N. acknowledges Jain University for providing financial support to carry out the research work.

References

[1] T.P. Yendrapati, K.V. Rao, V.S. Saikumar, B.S. Kumari, Adv. Nanopart. 2 (2013) 45–49.
[2] M.A. Ali, M.R. Idris, M.E. Quayum, J. Nanostruct. Chem. 3 (2003) 36–39.
[3] A. Rahman, R. Jayaganthan, R. Chandra, Mater. Sci. Semicond. Process. 18 (2014) 15–21.
[4] R. Georgekutty, M.K. Seery, S.C. Pillai, J. Phys. Chem. C 112 (2008) 13563–13570.
[5] X. Yin, W. Que, D. Fei, F. Shen, Q. Guo, J. Alloys Compd. 524 (2012) 13–21.
[6] A.B. Djuris, Y.H. Leung, C.H. Choy, K.W. Cheah, W.K. Chan, Appl. Phys. Lett. 84 (2004) 2635–2637.
[7] Y. Nosaka, Ohta Nobuhiro, Miyama Hajime, J. Phys. Chem. 9 (1990) 3152–3155.
[8] T.Y. Kim, J.Y. Kim, S.H. Lee, H.W. Shim, S.H. Lee, E.K. Suh, K.S. Nahma, Synth. Met. 144 (2004) 61–68.
[9] N.F. Djaja, R. Saleh, Mater. Sci. Appl. 4 (2013) 145–152.
[10] J. BandaraH. Weerasinghe, Sol. Energy Mater. Sol. Cells 85 (2005) 385–390.
[11] M. Ahmad, E. Ahmed, Y. Zhang, Z. Hong, Curr. Appl. Phys. 13 (2013) 697–704.
[12] N. Assi, M. Sharif, H. Bakhtiari, M. Naeini, Int. J. Nano Dimens. 5 (2014) 145–154.
[13] R.B. Reed, D.A. Ladner, J.F. Ravvile, Environ. Toxicol. Chem. 31 (2012) 93–99.
[14] L. Gao, S.T. Yang, S. Li, Y. Meng, H. Wang, H. Lei, J. Appl. Toxicol. 33 (2013) 1079–1088.
[15] F. Mohamad, Eur. J. Exp. Biol. 3 (2013) 97–103.
[16] O. Bondarenko, K. Juganson, A. Ivask, A. Kahru, Arch. Toxicol. 87 (2013) 1181–1200.
[17] S. Azizi, M.B. Ahamad, M.Z. Hussein, N.A. Ibrahim, Molecules 18 (2013) 6269–6280.
[18] M.A. Rahman, S. Mahmud, A.K. Alias, A.F. Nor., J. Phys. Sci. 17 (2013) 24–38.
[19] O. Altıntas Yıldırım, H.E. Unalan, C. Durucan, J. Am. Ceram. Soc. 96 (2013) 766–773.
[20] T. Wang, Z. Jiao, T. Chen, Y. Li, W. Ren, S.Y. Bi, Nanoscale 5 (2013) 7552–7557.
[21] P.V. Kamat, Chem. Rev. 93 (1993) 267–300.
[22] A.H. Shah, E. Manikandan, V. Ganesan, J. Nanomed. Nanotechnol. 2 (2013) 4–8.
[23] C. Karunakaran, V. Rajeswari, P. Gomathisankar, Mater. Sci. Semiocond. Process. 14 (2001) 133–138.
[24] F. Meng, H. Lu, ISRN Metallurgy Article ID 429818, 2013.
[25] F. Meng, H. Lu, Adv. Eng. Mater. 11 (2009) 198–201.
[26] R. Wang, J.H. Xin, Y. Yang, H. Liu, L. Xu, J.Hu, J. Appl. Surf. Sci. 227 (2004) 312–317.
[27] T. Jan, J. Iqbal, M. Ismail, M. Zakaullah, S.H. Naqvi, N. Badshah, Int. J. Nanomed. 9 (2013) 3679–3687.
[28] G. Nagaraju, T.N. Ravishankar, K. Manjunatha, S. Sarkar, H. Nagabhushana, R. Goncalves, J. Dupont, Mater. Lett. 109 (2013) 27–30.
[29] K. Namratha, K. Byrappa, J.Bai, J. Biomater. Tissue Eng. 33 (2013) 190–195.
[30] P.S. Sathish Kumar, A. Manivel, S. Anandan, Water Sci. Technol. 59 (2009) 1423–1430.
[31] X. Li, Y. Wang, J. Alloys Compd. 509 (2011) 5765–5768.
[32] B.M. Nagabhushana, R.P. Sreekanth, K.P. Ramesh, C. Shivakumara, G. T. Chandrappa, Mater. Res. Bull. 41 (2006) 1735–1746.
[33] K.C. Patil, S.T. Aruna, T. Mimani, Curr.Opin. Solid State Mater. Sci. 6 (2002) 507–512.
[34] N.K. Daud, B.H. Hameed, Desalination Water Treat. 37 (2012) 1–7.
[35] R. Wahab, S.G. Ansari, K. Seo, G.S. Kim, Mater. Res. Bull. 42 (2007) 1640–1648.
[36] T.K. Gupta, P.L. Hower, J. Appl. Phys. 50 (1992) 4849–4853.
[37] K. Nejati, Z. Rezvani, R. Pakizevand, Int. Nano Lett. 1 (2011) 75–81.

[38] G. Shan, L. Xu, G. Wang, Y. Liu, J. Phys. Chem. C 111 (2007) 3290–3293.
[39] K. Sarvari, A. Gangly, T. Ahamd, Bull. Mater. Sci. 35 (2012) 377–381.
[40] M. Faisal, S.B. Khan, M.M. Rahman, A. Jama, Appl. Surf. Sci. 258 (2011) 672–677.
[41] S.B. Khan, M. Faisal, M.M. Rahman, A. Jamal, Talanta 85 (2011) 943–949.
[42] M. Faisal, S.B. Khan, M.M. Rahman, A. Jamal, Chem. Eng. 173 (2011) 178–184.
[43] M.M. Rahmanan, M. Faisal, ACS Appl. Mater. Interfaces 3 (2011) 1346–1351.
[44] E. Sumesh, M.S. Bootharaju, A.T. Pradeep, J. Hazard. Mater. 189 (2011) 450–457.
[45] Y. Lai, H. Zhang, K. Xie, D. Gong, Z. Chen, New J. Chem. 34 (2010) 1335–1340.
[46] A. Sharma, B.P. Sing, S. Dhar, A. Gondorf, M. Spasova, Surf. Sci. 13 (2013) 606–609.
[47] S. De, A. Layek, S. Bhattacharya, D.K. Das, A. Kadir, A. Bhattacharya, S. Dharand, A. Chowdhury, Appl. Phys. Lett. 101 (2012) 121919–121923.
[48] R.H. Heuberger, A. Rossian, N.D. Spencer, Biol. Lett. 3 (2007) 183–185.
[49] A.P. Dementjev, A. Graaf, M.C.M. van de Sanden, K.I. Maslakov, A.V. Naumkin, A.A. Serov, Diam. Relat. Mater. 9 (2000) 1904–1907.
[50] M. Gabás, S. Gota, J.R. Ramos, M. Sánchez, N.T. Barrett, J. Avila, M. Sacchi, Appl. Phys. Lett. 86 (2005) 042104–042107.
[51] Y. Altıntas, H.E. Emrah, D. Caner, J. Am. Ceram. Soc. 3 (2013) 766–769.
[52] A.H. Shah, E. Manikandan, M. Basheer, V. Ganesan, J. Nanomed. Nanotechnol. 3 (2013) 2–6.
[53] D. Qin, Y. Guangruiy, H.E.Z. Guox, Q. Zhang, L.I. Luyao, Chalcogenide Lett. 9 (2012) 441–443.
[54] N.P. Mohabansi, V.B. Patil, N.A. Yenkie, Rasayan J. Chem. 4 (2011) 814–817.
[55] K. Byrappa, A.K. Subramani, S. Ananda, K.M. Lokanatha Rai, M.H. Sunitha, Bull. Mater. Sci. (2007) 30–33.
[56] S. Likius, H. Daniel, N. Nagai, M. Yoshida, Sato, Catalysts 3 (2013) 625–645.
[57] B.N. Patil, D.B. Nayak, V.S. Shrivastava, J. Appl. Chem. Res. 13 (2010) 13–17.
[58] L. Irimpan, V.P. Nampoori, P. Radhakrishnan, Chem. Phys. Lett. 455 (2008) 265–269.
[59] K.M. Joshi, V.S. Shrivatava, Int. J. Nano Dimens. 2 (2012) 241–252.